Visual Vibrometry: Estimating Material Properties from Small Motions in Video

Abe Davis*, Katherine L. Bouman*, Justin G. Chen, Michael Rubinstein, Oral Büyüköztürk, Frédo Durand, and William T. Freeman

1 Rods

1.1 Additional Results

In this section we provide our estimated Young's modulus for each rod along with the recovered resonant frequencies and corresponding mode visualizations. The estimated Young's modulus values for each of the rods can be seen in Table 3. We compare each of the estimated values to the manufacturer's reported Young's modulus. Since the material properties of birch and fiberglass are quite variable depending on the shipment, no material property values were reported for these rods.

	REPORTED	22 INCH	15 INCH
BRASS	1.4000×10^7	1.4134×10^7	1.3106×10^7
COPPER	1.7000×10^7	1.6747×10^7	1.6149×10^7
ALUMINUM	1.0000×10^7	0.9106×10^7	0.7741×10^7
STEEL	2.9000×10^7	2.5818×10^7	2.4625×10^7
BIRCH	–	0.3151×10^7	0.3214×10^7
FIBERGLASS	–	0.4241×10^7	0.4185×10^7

Table 1: Our estimated and the corresponding reported (from the manufacturer) Young's Modulus for each rod. For each of the six rods we estimated the Young's modulus when they were clamped at 2 different lengths: 22 and 15 inches. Since we know the geometry and the density of the rods, we are able to solve for the Young's modulus using the equations provided in the paper.

Recovering the Young's Modulus of a rod from video requires that we first identify the resonant frequencies. The voting scheme described in the paper was used to identify the resonant frequencies of each rod. The recovered frequencies can be seen in Tables 2 and 3 for the 22 and 15 inch clamped rods respectively. The visualized spatial phase patterns corresponding to each recovered resonant frequency is also shown. A colorwheel indicating the map between phase/amplitude and color in these visualizations can be seen in Figure 1b. Our recovered spatial phase visualizations correspond well with the theoretical mode shapes (Figure 1a), suggesting we are identifying the correct resonant frequencies for most of the clamped rods. Figure 4 shows the power spectra and recovered resonant frequencies for each of the rod videos.

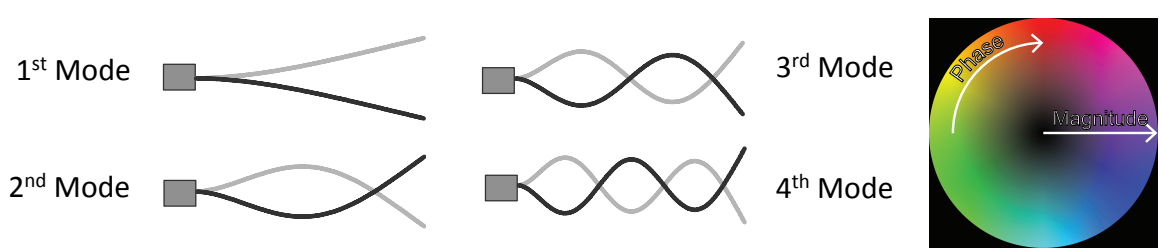

(a) Theoretical Mode Shapes (b) Color Wheel

Figure 1: (A) The theoretical mode shapes of a clamped rod. (B) Spatial Phase Visualization Color Wheel. Phase (motion direction) is mapped to hue and amplitude is mapped to saturation in our spatial phase visualizations.

*Joint First Author

	MODE NUMBER	FREQUENCY (HZ)	SPATIAL PHASE VISUALIZATIONS
BRASS	1	4.8046	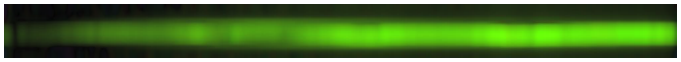
	2	30.3148	
	3	85.0531	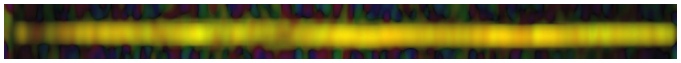
	4	166.6743	
COPPER	1	5.0906	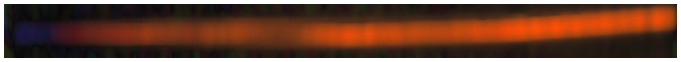
	2	32.1451	
	3	90.0293	
	4	176.4551	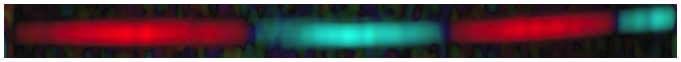
ALUMINUM	1	6.8637	
	2	43.3559	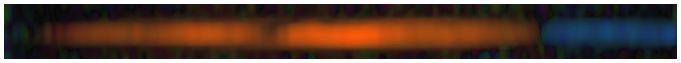
	3	121.4881	
	4	238.1715	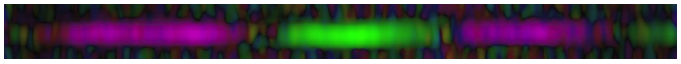
STEEL	1	6.8065	
	2	42.8411	
	3	120.0009	
	4	235.2544	
BIRCH	1	8.0649	
	2	49.9337	
	3	139.7913	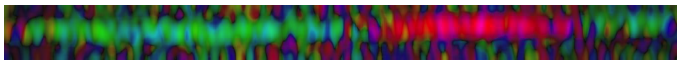
	4	274.0917	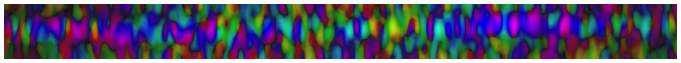
FIBERGLASS	1	5.3766	
	2	34.3615	
	3	96.0351	
	4	188.1235	

Figure 2: **22 inch rods:** The first 4 resonant frequencies, corresponding to modes 1-4, were recovered for each 22 inch rod using the voting method described in the paper. For each recovered resonant frequency, a visualization spatial phase patterns are shown. Note that changes in color correspond to changes in the direction of motion for the theoretical mode shapes. This verifies that our voting scheme is recovering the modes of the clamped rod.

	MODE NUMBER	FREQUENCY (HZ)	SPATIAL PHASE VISUALIZATIONS
BRASS	1	9.9524	
	2	62.5744	
	3	175.1968	
	4	343.4154	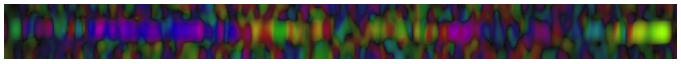
COPPER	1	10.7532	
	2	67.5506	
	3	189.2102	
	4	370.8703	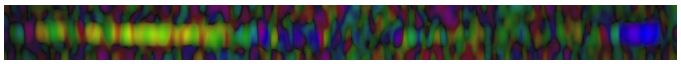
ALUMINUM	1	13.6131	
	2	85.6823	
	3	239.8874	
	4	470.1656	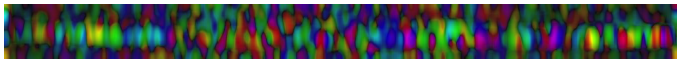
STEEL	1	14.2994	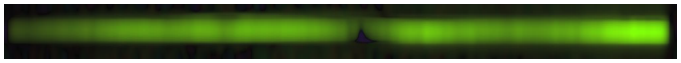
	2	90.0293	
	3	252.1278	
	4	494.0743	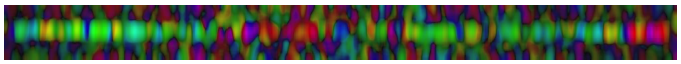
BIRCH	1	17.2165	
	2	108.733	
	3	303.7201	
	4	595.5431	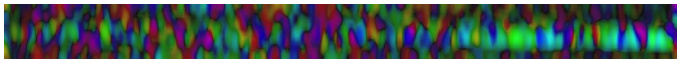
FIBERGLASS	1	11.6111	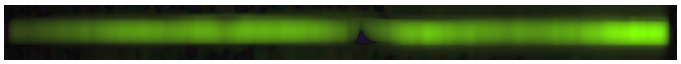
	2	73.213	
	3	205.1684	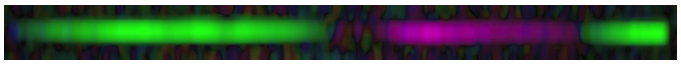
	4	401.6427	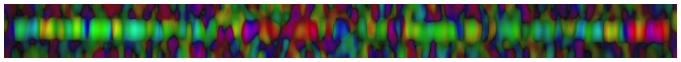

Figure 3: **15 inch rods:** The first 4 resonant frequencies, corresponding to modes 1-4, were recovered for each 15 inch rod using the voting method described in the paper. For each recovered resonant frequency, a visualization spatial phase patterns are shown. Note that changes in color correspond to changes in the direction of motion for the theoretical mode shapes. This verifies that our voting scheme is recovering the modes of the clamped rod. Mode visualizations are noisier for the 15 inch rods compared to the 22 inch rods because the corresponding resonant frequencies are higher.

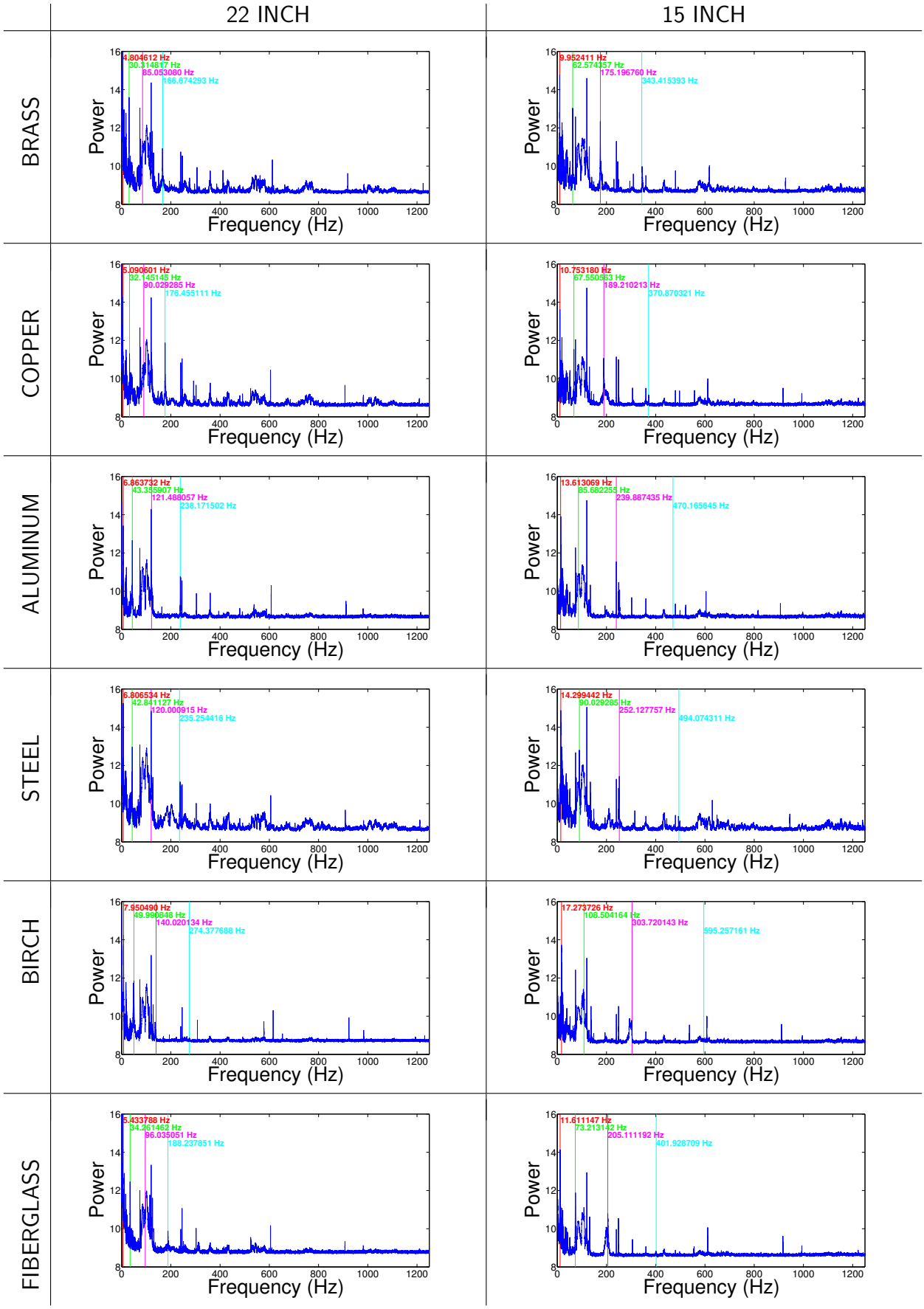

Figure 4: The extracted power spectrum for each rod video. Each power spectrum is labeled with the first 4 recovered resonant frequencies (red = 1st mode, green = 2nd mode, magenta = 3rd mode, cyan = 4th mode). These resonant frequencies are used to estimate the material properties of the rod.

1.2 Error Propagation for Density and Young's Modulus Calculations

Error propagation for the density and Young's Modulus calculations are done using the accepted method assuming independent variables [2]. Given a function $F(a, b, c, ...)$, the equation for the error σ_F depending on the errors $\sigma_a, \sigma_b, \sigma_c...$ is as follows:

$$\sigma_F = \sqrt{\left(\frac{\partial F}{\partial a}\right)^2 \sigma_a^2 + \left(\frac{\partial F}{\partial b}\right)^2 \sigma_b^2 + \left(\frac{\partial F}{\partial c}\right)^2 \sigma_c^2 + ...} \tag{1}$$

Density measurements were made by weighing the rods on a scale to obtain the mass m, measuring the length l of the rods, and using the specified diameter d. The error on the density was found by propagating the errors for the mass, length, and reported tolerances for the rod diameter.

$$\rho = \frac{4 * m}{\pi * l * d^2} \tag{2}$$

$$\sigma_\rho = \sqrt{\left(\frac{\rho}{m}\right)^2 \sigma_m^2 + \left(\frac{\rho}{l}\right)^2 \sigma_l^2 + 4\left(\frac{\rho}{d}\right)^2 \sigma_d^2} \tag{3}$$

The resulting densities of the materials are given in Table 2 with error bounds and comparison to the reported values.

Material	**Measured ρ**	**Measured σ_ρ**	**Reported ρ**
Steel	0.2808	0.00450	0.284
Aluminum	0.09740	0.00935	0.097-0.1
Copper	0.3256	0.0104	0.321-0.323
Brass	0.3085	0.0148	0.307
Birch	0.02512	0.00281	0.0224
Fiberglass	0.07237	0.00116	0.063

Table 2: Comparison between measured and reported density values all in units of lb/cu in

The Young's Modulus was calculated from the first resonant frequency f_1, density ρ, rod length l, rod diameter d, and a constant C of 0.1399 for the first resonant mode. The calcualted error for Young's Modulus then depended on the errors for the density, length, and diameter.

$$E = \rho\left(\frac{f_1^2 l^4}{C^2 d^2}\right) \tag{4}$$

$$\sigma_E = \sqrt{4\left(\frac{E}{d}\right)^2 \sigma_d^2 + 16\left(\frac{E}{l}\right)^2 \sigma_l^2 + \left(\frac{E}{\rho}\right)^2 \sigma_\rho^2} \tag{5}$$

2 Fabrics

2.1 PLSR vs PCR

Two standard regression methods modeling the relationship between the power spectra and material properties have been explored: Principal Components Regression (PCR) and Partial Least Squares Regression (PLSR). Both methods perform comparably, suggesting that the power of our algorithm is in the features, the processed power spectrum, rather than the regression model. Results comparing PLSR and PCR can be seen in Figure 5 for fabric stiffness, and Figure 6 for fabric area weight.

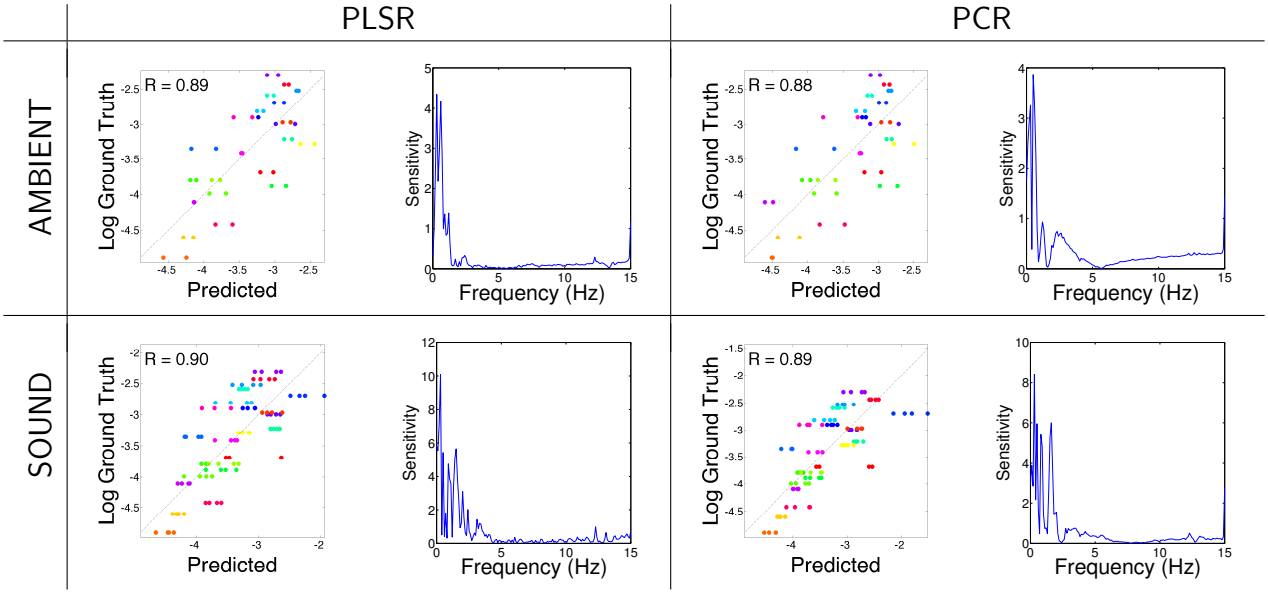

Figure 5: **Stiffness:** Comparisons between ground truth and the PLSR or PCR model predictions of fabric stiffness estimated from videos of fabric excited by ambient forces and acoustic waves. Both methods perform comparably, suggesting that the power of our algorithm is in the features, the processed power spectrum, rather than the regression model.

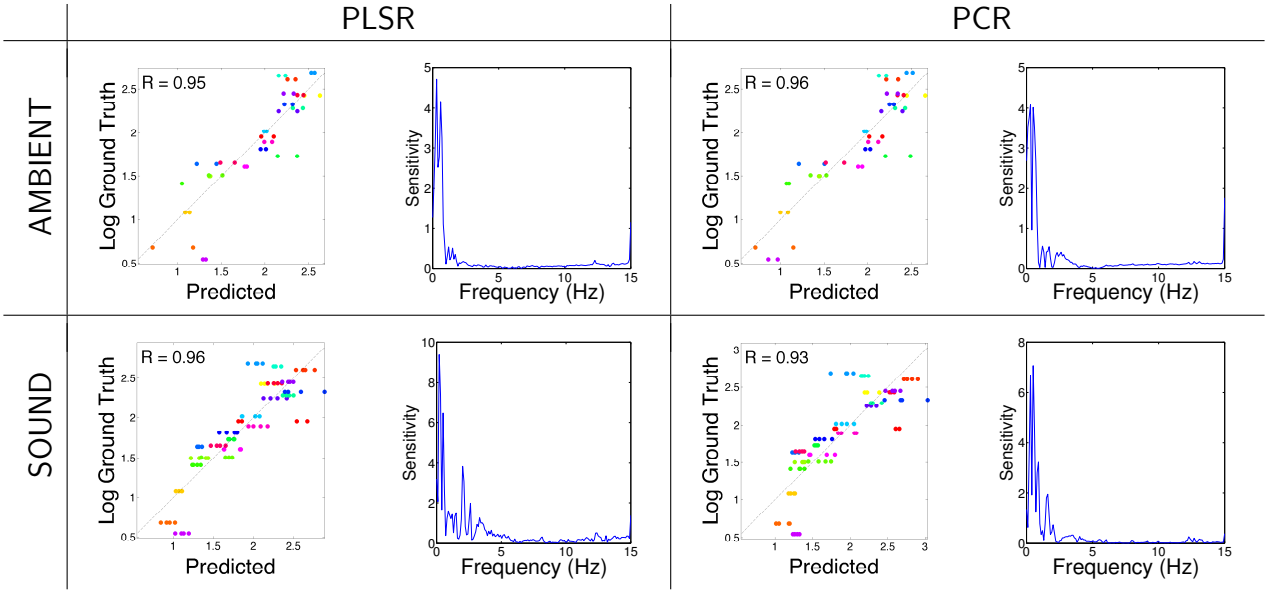

Figure 6: **Area Weight:** Comparisons between ground truth and the PLSR or PCR model predictions of fabric area weight estimated from videos of fabric excited by ambient forces and acoustic waves. Both methods perform comparably, suggesting that the power of our algorithm is in the features, the processed power spectrum, rather than the regression model.

	PLSR AMBIENT	PLSR SOUND	PCR AMBIENT	PCR SOUND
STIFFNESS	R=0.89 %=12.3 τ=0.70	R=0.90 %=12.5 τ=0.74	R=0.88 %=13.0 τ=0.67	R=0.89 %=12.5 τ=0.77
AREA WEIGHT	R=0.95 %=15.7 τ=0.86	R=0.96 %=13.3 τ=0.85	R=0.89 %=13.0 τ=0.84	R=0.93 %=17.8 τ=0.82

Table 3: The Pearson correlation value (R), Percentage Error (%), and Spearman Tau (τ) measures of performance for each model. The models were trained and tested separately on videos of fabric excited by acoustic waves (Sound) and ambient forces (Ambient).

2.2 Dimensionality Selection

Performance was evaluated using a varying number of components from PLSR or PCR. From this evaluation we chose a value, M, for the number of components that was both robust and results in good accuracy for both material properties. The Pearson correlation value as a function of the number of components used in the regression model (dimensionality) is shown in Figure 7. The red line indicates the M value selected for results presented in the paper and Figures 5, 6, and Tables 4, 5.

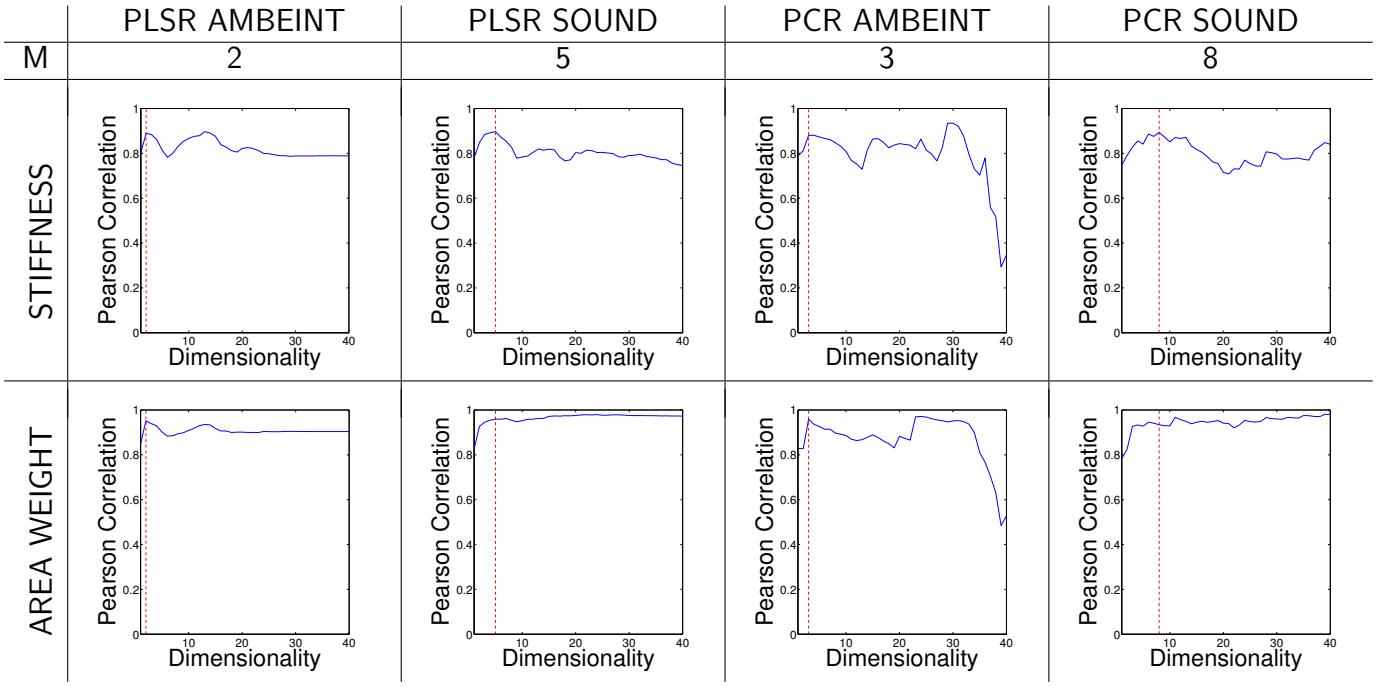

Figure 7: The Pearson product correlation value between predicted results and the ground truth measured properties when fitting a model with a varying number of components (dimensionality) is shown for each model. The number of components, M, was chosen for each model that resulted in good accuracy for both material properties. These selected values are shown above and are indicated on the plots as a vertical red line.

2.3 Additional Results

The average estimated material properties of the fabrics compared to measured ground truth values can be seen in Tables 4 and 5 for stiffness and area weight respectively. Models predicted the log of the material properties, but were inverted back to the original scale for results presented in these tables. Fabrics with inaccurate motion estimates due to specularities or the lack of texture were omitted (the same fabrics were omitted in [1]). These are identified by a dash in the prediction rows.

Description	Lycra	Faux Fur	Silk	Silk	Cotton
Bending Stiffness (lbf-in^2)	0.0250	0.0512	0.0075	0.0110	0.0100
Ambient Prediction	0.0444	0.0586	0.0122	–	0.0147
Sound Prediction	0.0467	0.0607	0.0114	–	0.0137
		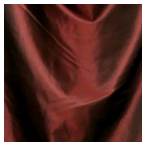			
Description	Wool	Taffeta	Linen	Corduroy	Cotton
Bending Stiffness (lbf-in^2)	0.0375	0.0165	0.0225	0.0185	0.0225
Ambient Prediction	0.0788	–	0.0217	0.0222	0.0158
Sound Prediction	0.0399	–	0.0290	0.0197	0.0209
Description	Velvet	Fleece	Denim	Upholstery	Upholstery
Bending Stiffness (lbf-in^2)	0.0200	0.0205	0.0250	0.0400	0.0750
Ambient Prediction	–	0.0526	–	0.0599	0.0467
Sound Prediction	–	0.0278	–	0.0651	0.0389
Description	Pleather	Minky	Damask Upholstry	Flannel Backed Vinyl	Upholstry
Bending Stiffness (lbf-in^2)	0.1000	0.0600	0.0800	0.0350	0.0675
Ambient Prediction	–	0.0405	0.0684	0.0182	0.0528
Sound Prediction	–	0.0348	0.0414	0.0173	0.1047
Description	Outdoor Polyester	Silk	Wool	Canvas	Nylon Rip Stop
Bending Stiffness (lbf-in^2)	0.0550	0.0300	0.0500	0.1000	0.0165
Ambient Prediction	0.0394	–	0.0577	0.0482	0.0159
Sound Prediction	0.0435	–	0.0634	0.0584	0.0151
	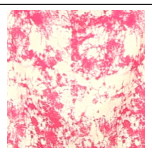				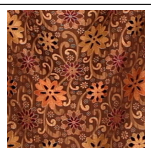
Description	Terry Knit	Lycra	Laminated Cotton	Lycra	Upholstry
Bending Stiffness (lbf-in^2)	0.0330	0.0550	0.0500	0.0120	0.0875
Ambient Prediction	0.0312	0.0317	–	0.0243	0.0585
Sound Prediction	0.0312	0.0250	–	0.0241	0.0549

Table 4: **Stiffness:** Measured stiffness for the 30 fabrics in the dataset and the corresponding average predicted stiffness across videos using a model fit to videos of fabric exposed to ambient forces or acoustic waves (sound).

Description	Lycra	Faux Fur	Silk	Silk	Cotton
Area Weight (oz/yd^2)	7.0600	13.5400	1.9750	2.6350	2.9400
Ambient Prediction	7.6123	10.0153	2.5742	–	3.0414
Sound Prediction	7.8031	15.2153	3.3750	–	3.4855
		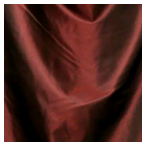			
Description	Wool	Taffeta	Linen	Corduroy	Cotton
Area Weight (oz/yd^2)	11.3400	3.3750	4.4750	4.5150	4.1045
Ambient Prediction	12.6974	–	3.9318	4.2042	2.8567
Sound Prediction	12.8771	–	3.2966	5.6169	3.5995
Description	Velvet	Fleece	Denim	Upholstery	Upholstery
Area Weight (oz/yd^2)	3.9250	5.6300	8.7500	9.8100	14.1600
Ambient Prediction	–	9.5621	–	10.7683	8.9886
Sound Prediction	–	7.1749	–	8.8255	9.6598
Description	Pleather	Minky	Damask Upholstry	Flannel Backed Vinyl	Upholstry
Area Weight (oz/yd^2)	16.6600	7.5100	14.6650	5.1400	10.2570
Ambient Prediction	–	7.4278	12.8091	3.7907	9.6775
Sound Prediction	–	8.3077	5.8836	3.5458	9.9868
Description	Outdoor Polyester	Silk	Wool	Canvas	Nylon Rip Stop
Area Weight (oz/yd^2)	6.1100	4.0935	9.4600	11.5900	1.7261
Ambient Prediction	7.2459	–	9.6180	9.6990	3.6910
Sound Prediction	4.8851	–	10.7175	11.3958	3.7694
	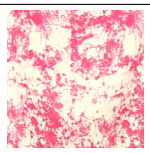				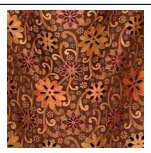
Description	Terry Knit	Lycra	Laminated Cotton	Lycra	Upholstry
Area Weight (oz/yd^2)	4.9850	6.6400	5.3200	5.2100	11.3900
Ambient Prediction	5.9321	7.6745	–	4.8186	11.1042
Sound Prediction	5.6753	5.7562	–	4.7737	10.6171

Table 5: **Area Weight:** Measured area weight for the 30 fabrics in the dataset and the corresponding average predicted area weight across videos using a model fit to videos of fabric exposed to ambient forces or acoustic waves (sound).

References

[1] K. L. Bouman, B. Xiao, P. Battaglia, and W. T. Freeman. Estimating the material properties of fabric from video. *Computer Vision, IEEE International Conference on*, 0:1984–1991, 2013.

[2] H. Ku. Notes on the use of propagation of error formulas. *Journal of Research of the National Bureau of Standards*, 70(4), 1966.

[3] J. Portilla and E. P. Simoncelli. A parametric texture model based on joint statistics of complex wavelet coefficients. *Int. J. Comput. Vision*, 40(1):49–70, Oct. 2000.